View metadata, citation and similar papers at core.ac.uk

brought to you by CORE

provided by Repository@USM

PA-MBE GaN-BASED OPTOELECTRONICS ON SILICON SUBSTRATES

CHUAH LEE SIANG

UNIVERSITI SAINS MALAYSIA

2009

PA-MBE GaN-BASED OPTOELECTRONICS ON SILICON SUBSTRATES

by

CHUAH LEE SIANG

Thesis submitted in fulfillment of the requirements for the degree of Doctor of Philosophy

2009

ACKNOWLEDGEMENTS

First of all, I would like to take this opportunity to express my sincere gratitude to my main supervisor, Prof. Dr. Zainuriah Hassan, for her valuable guidance and dedicated support throughout the course of this project, which had led to some successes like winning the Anugerah Sanggar Sanjung 2007, Hadiah Sanjungan 2007 and 2008 for Journal Publication Category. I would also like to thank my co-supervisor, Assoc. Prof. Dr. Haslan Abu Hassan for his enlightening ideas as well as his assistance and support to me throughout the course of my research project. Without them, this thesis would not have seen the light of day.

I would like to take this opportunity to thank NOR laboratory staffs for their generous help and technical support offered during my laboratorial work. Their commitments have indeed made this project able to be completed smoothly. Particularly important in this research project is my fellow buddy, Mr. Chin Che Woei. Also not to be forgotten are Dr. Ng Sha Shiong, Dr. Yam Fong Kwong, Dr. Magdy Hussien Mourad Mohamed, Dr. Naser Mahmoud Ahmed, Dr. Sabah M. Thahab, Mr. Sin Yew Keong and Mr. Naif Alhardan, for their sincere assistances in many areas such as sample preparation, technical paper writing, and experimental set up.

I would also like to gratefully acknowledge all staff members of the School of Physics and also USM Fellowship for supporting this work. Last but not least, I would like to thank my parents and family members for their love, encouragement, and support to me in my studies.

TABLE OF CONTENTS

	Page
ACKNOWLEDGEMENTS	ii
TABLE OF CONTENTS	iii
LIST OF TABLES	ix
LIST OF FIGURES	xi
LIST OF SYMBOLS	xvii
LIST OF MAJOR ABBREVIATIONS	xx
ABSTRAK	xxi
ABSTRACT	xxiii
CHAPTER 1 : INTRODUCTION	**1**
1.1 General properties of III-V nitrides	1
1.1.1 Crystal structure of group III-nitrides	3
1.1.2 Brief history of group III-nitrides	4
1.1.3 Doping of GaN	5
1.2 GaN-based optoelectronics on silicon substrates	7
1.2.1 LEDs on silicon substrates	8
1.2.2 Lasers on silicon substrates	9
1.2.3 Photodetectors on silicon substrates	12
1.3 Research objectives	13
1.3.1 Originality of the research works	15
1.4 Outline of the thesis	16
CHAPTER 2 : LITERATURE REVIEW	**17**
2.1 III-V nitrides growth techniques	17
2.1.1 Molecular beam epitaxy (MBE)	17
2.1.2 Metal-organic chemical vapour deposition (MOCVD)	19
2.2 Factors influencing GaN crystalline quality	21
2.2.1 Substrates	22
2.2.2 Buffer layer	26
2.3 III-V nitrides-based photodetectors	29
2.3.1 Types of photodetector	32
2.3.1.1 Photoconductive detector	32

2.3.1.2 p-n junction or p-i-n photodiode 33
2.3.1.3 Schottky barrier photodiode 35
2.3.1.4 Metal-semiconductor-metal (MSM) photodiode 37
2.4 Overview of metal-GaN contact technology 39
2.4.1 Theory of metal-semiconductor contact 39
2.4.2 Ohmic contact on GaN 41
2.4.3 Schottky contact on GaN 45
2.5 Development of porous GaN-based material 49
2.6 Principle of GaN-based devices 51
2.6.1 MSM photodetector 51
2.6.2 Heterojunction photodiodes 54

CHAPTER 3: GROWTH, CHARACTERIZATION AND FABRICATION METHODS 56

3.1 MBE system 57
3.1.1 MBE radio frequency (RF) plasma nitrogen source 58
3.1.2 MBE vacuum chamber 59
3.1.3 Effusion cells 61
3.1.4 Sample manipulation 62
3.2 Investigation of the desorption energy of Ga 63
3.2.1 Growth rate as a function of III and N fluxes 63
3.2.2 Surface morphology diagram for GaN 64
3.3 MBE growth kinetics 65
3.4 Principle of the characterization tools 68
3.4.1 RHEED 68
3.4.2 X-ray diffraction 71
3.4.3 Scanning electron microscopy 74
3.4.4 Energy dispersive X-rays analysis 76
3.4.5 Atomic force microscopy 78
3.4.6 Photoluminescence spectroscopy 80
3.4.7 Raman spectroscopy 82
3.4.8 Hall effect 83
3.4.9 Thin film thickness measurement – Filmetrics 87
3.5 Porous semiconductor generation mechanisms 88
3.6 Physical metal deposition 89
3.6.1 Metallization via thermal evaporation 89

3.6.2 Metallization via direct current (DC) sputtering 90

CHAPTER 4: METHODOLOGY **92**

4.1 Silicon substrate preparation and mounting 92
4.2 Flux optimization of the source materials 95
4.3 GaN-based materials 96
4.3.1 Growth conditions 96
4.3.1.1 GaN film on Si(111) 98
4.3.1.2 n- and p-doped GaN on Si(111) 99
4.3.1.3 $Al_{0.09}Ga_{0.91}N$ film on Si(111) 101
4.3.1.4 n-type $In_{0.47}Ga_{0.53}N$/GaN heterostructure on Si(111) 101
4.3.1.5 AlN cap layer/GaN on Si(111) 102
4.3.2 Characterization of epilayers 103
4.4 Porous GaN and porous $Al_{0.09}Ga_{0.91}N$ 103
4.4.1 Porous III-nitrides prepared by Pt assisted electroless etching 104
4.4.2 Characterization 104
4.5 Metal contacts 105
4.5.1 Wafer cleaning 105
4.5.2 Different types of metal contact studies and their characterizations 105
4.6 Fabrication and characterization of devices 107
4.6.1 MSM photodiode 107
4.6.1.1 Fabrication of MSM photodiode 107
4.6.1.2 Characterization of the MSM photodiode 110
4.6.2 Light emitting Schottky diodes 110
4.6.2.1 Fabrication of light emitting Schottky diodes 110
4.6.2.2 Probing condition 112
4.6.2.3 Characterization of light emitting Schottky diodes 112
4.6.3 GaN Schottky barrier photodiode with AlN cap layer 113
4.6.3.1 Fabrication of Schottky barrier photodiode 113
4.6.3.2 Characterization of Schottky barrier photodiode 113
4.6.4 p-GaN/n-Si heterojunction photodiode 113
4.6.4.1 Fabrication of heterojunction photodiode 114
4.6.4.2 Characterization of heterojunction photodiode 114
4.7 Summary 115

CHAPTER 5: THE STUDIES OF MATERIAL PROPERTIES **116**

5.1 Introduction 116
5.2 The study of GaN film on Si(111) 116
5.2.1 Hall effect measurement 116
5.2.2 Scanning electron microscopy and atomic force microscopy 116
5.2.3 Energy dispersive X-ray analysis 117
5.2.4 X-ray diffraction 118
5.2.5 Photoluminescence 120
5.2.6 Raman scattering 121
5.3 The study of n- and p-type GaN on Si(111) 123
5.3.1 Hall effect measurement 123
5.3.2 Scanning electron microscopy and atomic force microscopy 123
5.3.3 Energy dispersive X-ray analysis 125
5.3.4 X-ray diffraction 127
5.3.5 Photoluminescence 130
5.3.6 Raman scattering 131
5.4 The study of $Al_{0.09}Ga_{0.91}N$ film on Si(111) 134
5.4.1 Hall effect measurement 134
5.4.2 Scanning electron microscopy and atomic force microscopy 134
5.4.3 Energy dispersive X-ray analysis 135
5.4.4 X-ray diffraction 136
5.4.5 Photoluminescence 137
5.4.6 Raman scattering 138
5.5 The study of n-type $In_{0.47}Ga_{0.53}N$/GaN heterostructure on Si(111) 140
5.5.1 Hall effect measurement 140
5.5.2 Scanning electron microscopy and atomic force microscopy 140
5.5.3 Energy dispersive X-ray analysis 141
5.5.4 X-ray diffraction 141
5.5.5 Photoluminescence 144
5.5.6 Raman scattering 145
5.6 The study of AlN cap layer/GaN on Si(111) 146
5.6.1 Hall effect measurement 146
5.6.2 Scanning electron microscopy and atomic force microscopy 146
5.6.3 Energy dispersive X-ray analysis 147
5.6.4 X-ray diffraction 148

5.6.5 Photoluminescence 149
5.6.6 Raman scattering 150
5.7 Summary 151

CHAPTER 6: THE STUDIES OF POROUS GaN-BASED MATERIALS 154

6.1 Introduction 154
6.2 Porous GaN prepared by Pt-assisted electroless chemical etching 154
6.2.1 The study of porous GaN 154
6.2.1.1 Scanning electron microscopy and atomic force microscopy 154
6.2.1.2 High resolution XRD 157
6.2.1.3 Photoluminescence 159
6.2.2 The study of porous $Al_{0.09}Ga_{0.91}N$ 162
6.2.2.1 Scanning electron microscopy and atomic force microscopy 162
6.2.2.2 High resolution XRD 163
6.2.2.3 Photoluminescence 164
6.3 Summary 166

CHAPTER 7: THE STUDIES OF METAL CONTACTS 167

7.1 Introduction 167
7.2 The study of metal contacts on p-type GaN 167
7.2.1 Ni/Ag ohmic contacts on p-GaN 167
7.2.1.1 Specific contact resistivities 168
7.2.2 Ti- and Ag-based Schottky contacts on p-GaN 172
7.2.2.1 Electrical characteristics 172
7.3 The study of metal contacts (Ti, Ni, Ag, Pt) on n-GaN 175
7.3.1 Scanning electron microscopy 175
7.3.2 Energy dispersive X-ray spectroscopy 176
7.3.3 Current-voltage measurements 177
7.4 Summary 180

CHAPTER 8: THE STUDIES OF DEVICES 181

8.1 Introduction 181

8.2 Metal-semiconductor-metal (MSM) photodetectors 181
8.2.1 UV MSM photodetector based on porous GaN 182
8.2.1.1 Current-voltage measurements 182
8.2.1.2 Spectral responsivity 184
8.2.2 UV photodetector based on porous $Al_{0.09}Ga_{0.91}N$ 185
8.2.2.1 Current-voltage measurements 185
8.2.2.2 Spectral responsivity 188
8.2.3 $In_{0.47}Ga_{0.53}N$/GaN heterostructure for photodetector applications 189
8.2.3.1 Current-voltage measurements 189
8.2.3.2 Spectral responsivity 191
8.3 Red emission of thin film electroluminescent device based on p-GaN 192
8.3.1 Electrical characteristics 192
8.4 GaN Schottky barrier photodiode with AlN cap layer 196
8.4.1 Electrical characteristics 196
8.5 p-GaN/n-Si heterojunction photodiodes 202
8.5.1 Electrical characteristics 202
8.6 Summary 204

CHAPTER 9: CONCLUSIONS AND RECOMMENDATIONS FOR FUTURE RESEARCH **207**

9.1 Conclusions 207
9.2 Recommendations for future research 208

REFERENCES **211**

APPENDICES **232**
Appendix A: The fundamental properties of wurtzite III-nitride semiconductors at room temperature. 232
Appendix B: The Miller and Miller-Bravais indices 233
Appendix C: The Van Der Pauw technique 236

LIST OF PUBLICATIONS 239

LIST OF TABLES

		Page
Table 2.1:	Lattice parameters and thermal expansion coefficient of substrates. (data extracted from Popovici and Morkoc 2000)	23
Table 2.2:	Lattice mismatch between GaN and the substrates.	24
Table 2.3:	The overview of metal contacts/p-GaN.	42
Table 4.1:	Techniques used to analyze the samples.	103
Table 4.2:	Parameters of porous GaN-based generated by Pt-assisted electroless etching.	105
Table 4.3:	Scope of study, metal contacts, thermal treatment and characterization of p- and n-GaN samples.	107
Table 4.4:	Different probing conditions for samples.	112
Table 5.1:	Elements detected in the UID n-type GaN films by EDX and their corresponding weight and atomic composition.	118
Table 5.2:	Optical phonon modes (in cm^{-1}) of GaN/AlN/Si thin films obtained from Raman measurements.	123
Table 5.3:	Elements detected in the n- and p-doped GaN films by EDX and their corresponding weight and atomic composition.	127
Table 5.4:	Optical phonon modes (in cm^{-1}) of n-type GaN/AlN/Si thin films obtained from Raman measurements.	133
Table 5.5:	Optical phonon modes (in cm^{-1}) of p-type GaN/AlN/Si thin films obtained from Raman measurements.	134
Table 5.6:	Elements detected in the $Al_{0.09}Ga_{0.91}N$/AlN/Si(111) by EDX and their corresponding weight and atomic composition.	136
Table 5.7:	Optical phonon modes (in cm^{-1}) of $Al_{0.09}Ga_{0.91}N$ thin films obtained from Raman measurements.	139
Table 5.8:	Elements detected in the InGaN films by EDX and their corresponding weight and atomic composition.	141
Table 5.9:	Optical phonon modes (in cm^{-1}) of $In_{0.47}Ga_{0.53}N$/GaN/AlN/Si thin films obtained from Raman measurements.	146
Table 5.10:	Elements detected in the AlN cap layer/GaN films by EDX and their corresponding weight and atomic composition.	148

Table 5.11:	Optical phonon modes (in cm^{-1}) of AlN cap layer/GaN/AlN/Si thin film obtained from Raman measurements.	151
Table 5.12:	Summary of the characterization results of structural and optical properties of GaN-based films grown on silicon substrate.	153
Table 6.1:	The surface roughness (root mean square) of the samples measured by AFM on a 10 x 10 μm^2 scan area.	157
Table 6.2:	The diffraction peak positions of (0002) and ($10\bar{1}2$) planes, and lattice constants of different samples derived from XRD measurements.	158
Table 6.3:	The peak position, FWHM, peak shift and the relative intensity of near band edge PL of different samples.	160
Table 7.1:	The specific contact resistivities at different annealing temperatures and times.	170
Table 7.2:	EDX analysis data of oxygen for different samples under different annealing temperatures.	177
Table 8.1:	The ideality factor, SBH, dark and photo current of as grown and porous GaN photodetectors.	183
Table 8.2:	The ideality factor, SBH, dark and photo currents of as grown and porous $Al_{0.09}Ga_{0.91}N$ photodetectors.	186
Table 8.3:	Summary of the probing condition, the threshold voltage and SBH of samples.	195
Table 8.4:	Summary of the dark and photo current (I-V) characteristics of the samples annealed at different temperatures.	199
Table 8.5:	Summary of the ideality factor (*n*) and Schootky barrier height (SBH) of GaN-based photodetectors.	205
Table 8.6:	Summary of the dark and photo current (I-V) characteristics of the Ni/AlN/GaN/AlN Schottky barrier photodiodes annealed at different temperatures.	206

LIST OF FIGURES

		Page
Figure 1.1:	Bandgap energy versus effective lattice constant of nitride materials. (Popovici and Morkoc, 2000)	2
Figure 1.2:	The (a) wurtzite structure, and (b) zinc blende structure of III-V nitrides. (Detchprohm et al., 1992)	3
Figure 1.3:	Materials used in the demonstrations to date of lasers on Si and associated wavelength and emission color. Wavelength scale also indicates emission obtained from various REs in GaN (Steckl et al., 2007).	12
Figure 2.1:	Schematic diagram of growth chamber in a typical MBE system. (Sghaier et al., 2004)	18
Figure 2.2:	Diagram of a horizontal MOCVD reactor. (Morkoc, 1999)	21
Figure 2.3:	Solar UV irradiance at the top and the bottom of the earth's atmosphere. (Mayer et. al., 1999)	32
Figure 2.4:	(a) Photoconductor; (b) Simple structure of a photoconductor.	33
Figure 2.5:	(a) Schematic structure of a p-n junction photodiode; (b) schematic structure of a p-i-n photodiode.	34
Figure 2.6:	Absorption of photons by (a) band-to-band excitation and (b) internal photoemission. (Ng et. al., 2002)	36
Figure 2.7:	Schematic structure of a Schottky photodiode.	36
Figure 2.8:	An example of GaAs MSM-FET integration. (Makiuchi et. al., 1985)	37
Figure 2.9:	Two interdigitated Schottky contact pads connected back to back.	38
Figure 2.10:	The schematic top view of the MSM-PD with planar interdigitated electrodes.	38
Figure 2.11:	Schematic description of (a) the thermionic emission (TE), (b) thermionic field emission (TFE), and (c) tunneling mechanisms in an n-type semiconductor. Characteristics of (d) rectifying, (e) linear or ohmic I-V behavior. (Morkoc, 1999)	40
Figure 2.12:	(a) The transmission line pattern, (b) The typical graph showing the variation of the resistance with respect to the gap distance. (Morkoc, 1999)	44

Figure 2.13: Reported barrier heights of metals to n-GaN as a function of their work function. (adapted from Liu and Lau, 1998) 45

Figure 2.14: *I-V* characteristics of *In {I exp(qV/{kT})/[exp(qV/{kT})-1]} against V.* 49

Figure 2.15: (a) Representation of the interdigitated metallic finger structure of an MSM-photodiode. (b) cross-section through the physical layout. 52

Figure 3.1: Veeco Gen II molecular beam epitaxial (MBE) system. 57

Figure 3.2: Schematic illustration of the applied EPI UNI-bulb RF plasma source. 59

Figure 3.3: A schematic illustration of the kinetic processes that occur at the surface of the substrate during MBE growth. (Herman and Sitter, 1989) 66

Figure 3.4: Illustration of three distinct growth modes, (a) FM, (b) VW and (c) SK growth. (Herman and Sitter, 1989) 67

Figure 3.5: The configuration of the RHEED inside the MBE chamber. 68

Figure 3.6: RHEED patterns of GaN on Si(111): (a) RHEED pattern is spotty; (b) RHEED pattern is half streaky and half spotty; (c) RHEED pattern is streaky. 70

Figure 3.7: An illustration of the formation of a single monolayer as seen by a RHEED *in-situ* instrument. The corresponding RHEED oscillation signal is shown. (adapted from Ohring, 1992) 70

Figure 3.8: X-ray diffraction from two parallel atomic planes in a crystalline material. 72

Figure 3.9: Basic features of a typical XRD experiment. (Fewster, 2003) 74

Figure 3.10: The schematic diagram of a scanning electron microscope. (Schroder, 1998) 75

Figure 3.11: Elements in an EDX spectrum are identified based on the energy content of the X-rays emitted by their electrons as these electrons transfer from a higher-energy shell to a lower-energy one. (Manual of Thermo Scientific) 77

Figure 3.12: An example of EDX spectrum from the EDX measurements of AlGaN. 77

Figure 3.13: The fiber interferometer setup for AFM. (Operating manual, surface imaging system, 1999) 79

Figure 3.14: Simplified schematic of a typical PL setup. (Gfroerer et al., 2000). 81

Figure 3.15: Hall Effect experienced by an electron as it moves along a conductor or semiconductor perpendicularly to a magnetic field. (McGrath, 2001) 87

Figure 3.16: The Filmetrics F20 system. 88

Figure 3.17: Simplified diagram of an evaporator. (Wood et al., 1994) 90

Figure 3.18: Simplified diagram of the sputtering system used. (Wood et al., 1994) 91

Figure 4.1: Illustration of mounting a quarter of 3 inch silicon substrate on sample holder. 93

Figure 4.2: Illustration of combination of sample holder and substrate transfer arm. 94

Figure 4.3: Illustration of the substrate transferring from the sample holder combined with the substrate transfer arm to the substrate holder on CAR. 94

Figure 4.4: RHEED pattern of Si(111) 7×7 surface reconstruction pattern. 95

Figure 4.5: The beam equivalent pressures (BEP) of various elemental sources at different temperatures. 96

Figure 4.6: Flow chart of growth processes for six samples. 97

Figure 4.7: RHEED diffraction indicates clean Si(111) surface with prominent Kikuchi lines. 98

Figure 4.8: (a) Typical RHEED image at few monolayers of Al before AlN buffer layer growth; (b)-(d) show the RHEED images with 90 sec, 5 min and 15 min of AlN layers. 99

Figure 4.9: The electroless chemical etching experimental set up used to generate porous GaN. 104

Figure 4.10: Schematic diagram of the interdigitated Schottky contact for photodetector. 108

Figure 4.11: A simple electrical equivalent circuit of the photodiode. 109

Figure 4.12: A schematic cross section of the typical set up of the spectral response measurement of the GaN-based MSM PD. 110

Figure 4.13:	(a) Top view, (b) cross section view of ohmic and Schottky contacts of a typical Schottky diode sample.	111
Figure 5.1:	A typical SEM image of unintentionally doped n-type GaN on Si(111).	117
Figure 5.2:	A typical AFM image presenting the top surface morphology of UID n-type GaN/AlN/Si(111).	117
Figure 5.3:	Typical EDX spectrum of the UID n-type GaN/AlN/Si.	118
Figure 5.4:	XRD scan of UID n-type GaN/AlN/Si.	119
Figure 5.5:	XRD rocking curve of (0002) plane for UID n-type GaN/AlN/Si.	119
Figure 5.6:	Room temperature micro-PL spectrum of GaN on silicon.	120
Figure 5.7:	Room temperature micro-Raman spectra of the sample in the $z(x, \text{unpolarized})\bar{z}$.	122
Figure 5.8:	SEM images of (a) sample I and (b) sample II.	124
Figure 5.9:	AFM images presenting the top surface morphology of (a) sample I and (b) sample II.	125
Figure 5.10:	EDX spectrum of Si doped GaN/AlN/Si.	126
Figure 5.11:	EDX spectrum of Mg doped GaN/AlN/Si.	126
Figure 5.12:	XRD scan of GaN on AlN on Si: (a) sample I and (b) sample II.	128
Figure 5.13:	XRD RC of (0002) plane for UID, n- and p-GaN grown on Si substrate	129
Figure 5.14:	Room temperature PL spectrum of UID, n- and p-GaN on silicon.	131
Figure 5.15:	Room temperature micro-Raman spectra of UID, n- and p-GaN grown on silicon substrate.	132
Figure 5.16:	SEM images of the $Al_{0.09}Ga_{0.91}N$/AlN on Si substrate.	135
Figure 5.17:	AFM images presenting the top surface morphology of sample.	135
Figure 5.18:	EDX spectrum of the $Al_{0.09}Ga_{0.91}N$/AlN on Si(111).	135

Figure 5.19: (a) X-ray diffraction rocking curve (RC) of (0002) plane for $Al_{0.09}Ga_{0.91}N$/AlN on Si substrate and (b) Experimental data and best-fit simulated profile. 136

Figure 5.20: Room temperature micro-PL spectrum of $Al_{0.09}Ga_{0.91}N$ on silicon. 138

Figure 5.21: Room temperature Raman spectra of $Al_{0.09}Ga_{0.91}N$/AlN/Si sample measured with $z(x, \text{unpolarized})\bar{z}$ scattering configuration. 139

Figure 5.22: SEM images of the $In_{0.47}Ga_{0.53}N$/GaN heterostructure on Si(111). 140

Figure 5.23: AFM images of $In_{0.47}Ga_{0.53}N$/GaN heterostructure on Si(111). 140

Figure 5.24: EDX spectrum of the sample. 141

Figure 5.25: XRD spectrum of the InGaN/GaN/AlN/Si sample. 142

Figure 5.26: (a) X-ray diffraction RC of (0002) plane for $In_{0.47}Ga_{0.53}N$/GaN and (b) Experimental data and best-fit simulated profile. 142

Figure 5.27: PL spectra of the $In_{0.47}Ga_{0.53}N$/GaN/AlN/Si sample. 145

Figure 5.28: Room temperature Raman spectra of $In_{0.47}Ga_{0.53}N$/GaN/AlN/Si sample measured with $z(x, \text{unpolarized})\bar{z}$ scattering configuration. 145

Figure 5.29: SEM image of the AlN cap layer/GaN film on Si. 147

Figure 5.30: AFM image of AlN cap layer/GaN film on Si. 147

Figure 5.31: EDX spectrum of the AlN cap layer/GaN sample. 147

Figure 5.32: XRD scan of AlN/GaN/AlN/Si. 148

Figure 5.33: XRD rocking curve (RC) of (0002) plane for AlN/GaN/AlN/Si. 149

Figure 5.34: PL spectra of the AlN cap layer/GaN/AlN/Si sample. 149

Figure 5.35: Room temperature Raman spectra of AlN/GaN/AlN/Si sample measured with $z(x, \text{unpolarized})\bar{z}$ scattering configuration. 150

Figure 6.1: SEM images of the samples. (a) as grown, (b) etched for 10 min, (c) etched for 25 min, (d) etched for 35 min. 155

Figure 6.2:	AFM images of the porous GaN samples showing different surface topography. (a) as grown, (b) etched for 10 min, (c) etched for 25 min, (d) etched for 35 min.	156
Figure 6.3:	The near band edge PL spectra of samples etched under different durations.	160
Figure 6.4:	SEM images of the $Al_{0.09}Ga_{0.91}N$ samples. (a) as grown, (b) etched for 15 min.	162
Figure 6.5:	AFM micrographs of the $Al_{0.09}Ga_{0.91}N$ samples. (a) as grown, (b) etched for 15 min.	163
Figure 6.6:	HRXRD RC of (0002) plane for as grown and porous $Al_{0.09}Ga_{0.91}N$ grown on Si(111) substrates.	164
Figure 6.7:	The near band edge PL spectra of the $Al_{0.09}Ga_{0.91}N$ samples measured at room temperature: as grown and etched under 15 min.	165
Figure 7.1:	The changes of specific contact resistivities at different annealing temperatures.	169
Figure 7.2:	SEM images taken at different annealing temperatures.	171
Figure 7.3:	The I-V characteristics of Schottky contacts on p-GaN (a) before heat treatment, and (b) after heat treatment.	173
Figure 7.4:	SEM images of different samples annealed at 700 °C for 15 minutes: (a) Ni, (b) Ag (c) Pt and (d) Ti.	176
Figure 7.5:	The I-V characteristics of different samples: (a) as-deposited, (b) annealed at 300 °C, (c) annealed at 400 °C; and (d) annealed at 500 °C.	179
Figure 8.1:	The I-V characteristics of as grown and porous GaN photodetectors.	183
Figure 8.2:	The responsivity as a function of wavelength for MSM detector: (a) as grown, (b) porous GaN.	184
Figure 8.3:	The I-V characteristics of as grown and porous $Al_{0.09}Ga_{0.91}N$ photodetectors.	187
Figure 8.4:	The responsivity as a function of wavelength for MSM detector: (a) as grown, (b) porous AlGaN.	188
Figure 8.5:	I-V characteristics of the MSM photodiode under dark condition.	190

Figure 8.6:	Responsivity of $In_{0.47}Ga_{0.53}N$ MSM photodetector.	191
Figure 8.7:	The I-V characteristics of the samples with Schottky contacts made of In under three different probing conditions.	193
Figure 8.8:	A red emission produced by thin film electroluminescent device based on p-GaN.	195
Figure 8.9:	I-V characteristics of the fabricated photodiodes annealed at different temperatures: (a) as deposited, (b) 500 ºC, (c) 600 ºC and (d) 700 ºC.	198
Figure 8.10:	The I-V characteristics of p-GaN/n-Si photodiodes. Photo-currents under illumination (light) are shown from the diodes. Dark current behavior is also indicated as a reference. The inset shows I-V characteristics of the heterojunction in dark at room temperature.	204

LIST OF SYMBOLS

Symbol	Description
A^*	Effective Richardson constant
A_n^*	Effective Richardson constant for the electron
A_p^*	Effective Richardson constant for the hole
B	Magnetic field
b	Bowing factor
c	Speed of light
d	Interatomic spacing in a crystal lattice
E	Electric field
e	Charge of an electron
E_C	Conduction band
E_F	Fermi level of semiconductor
E_{Fm}	Fermi level of metal
E_g	Semiconductor band gap
E_V	Valence band
F	Force
G	Conductance
$g(E)$	Density of states
h	Planck's constant
I	Electric current
I_0	Saturation current
J	Current density
J_0	Saturation current density
k	Boltzmann constant
L_D	Traced length on the imaging screen (CRT display) of the SEM
L_S	Length of the scanned sample in the SEM
M	Magnification of the SEM
m^*	Effective electron mass
m_0	Free electron mass
n	Ideality factor
n	Refractive index
$N(E_F)$	Density of states at the Fermi level of semiconductor
NEP	Noise equivalent power
p	Hole carrier density
p_0	Equilibrium hole carrier density
q	Magnitude of the electronic charge
R	Resistance
R_H	Hall coefficient
S	Schottky contact area of the Schottky diode
T	Absolute temperature
v	Carriers drift velocity
V	Voltage
V_0	Contact potential of a metal-semiconductor or a p-n junction
V_e	Electron acceleration voltage
V_H	Hall voltage
V_r	Reverse bias voltage
$<v_x>$	Net drift velocity in the *x*-direction
W	Depletion region
α	Thermal expansion coefficient
β	Half width of the X-ray diffraction peak
θ	X-ray diffraction angle
ρ	Resistivity

σ	Conductivity
Φ_B	Schottky barrier height
Φ_{Bn}	Barrier height for electron
Φ_{Bp}	Barrier height for hole
Φ_m	Metal work function
Φ_s	Semiconductor work function
χ	Electron affinity

LIST OF MAJOR ABBREVIATIONS

2D	Two Dimensional
a.u.	Arbitrary Unit
AFM	Atomic Force Microscopy
BFM	Beam flux monitor
CTLM	Circular TLM
CRT	Cathode Ray Tube
CVD	Chemical vapor deposition
DAP	Donor-acceptor pair
DBE	Donor bound exciton
DC	Direct current
EDX	Energy dispersive X-ray analysis
ELDs	Electroluminescent devices
FET	Field-effect transistor
FE	Field emission
FWHM	Full width at half maximum
HEMT	High electron mobility transistor
HF	Hydrofluoric
HVPE	Hydride vapour phase epitaxy
IR	Infrared
I-V	Current-voltage
LD	Laser diode
LED	Light Emitting Diode
LEEBI	Low-energy electron-beam irradiation
LO	Longitudinal optical
MBE	Molecular beam epitaxy
MIS	Metal-insulator-semiconductor
MOCVD	Metalorganic chemical vapor deposition
MHz	Megahertz
MSM	Metal-semiconductor-metal
PA	Plasma-assisted
PBN	Pyrolytic boron nitride
PL	Photoluminescence
RF	Radio frequency
RCA	Radio Corporation of America
RHEED	Reflection high energy electron diffraction
rms	Root mean square
SBH	Schottky barrier height
SCR	Specific contact resistivity
TLM	Transmission line model
TMA	Trimethylaluminium
TMG	Trimethylgallium
TMI	Trimethylindium
UHV	Ultra-high vacuum
UV	Ultraviolet
VUV	Vacuum ultraviolet
XRD	X-ray diffraction

OPTOELEKTRONIK BERASASKAN GaN PA-MBE ATAS SUBSTRAT SILIKON

ABSTRAK

Dalam penyelidikan ini, epitaksi alur molekul berbantukan plasma nitrogen frekuensi radio (RF) digunakan untuk menumbuhkan bahan galium nitrid (GaN) di atas substrat Si(111) dengan penggunaan aluminium nitrid (AlN) yang ditumbuhkan pada suhu tinggi sebagai lapisan penimbal. Sepanjang proses pertumbuhan, pengedopan dilakukan dengan menggunakan Si dan Mg dengan ketulenen tinggi sebagai pendopan jenis-n dan jenis-p masing-masing. Sejumlah tujuh teknik telah digunakan untuk mengkaji ciri-ciri filem berasaskan GaN (jenis-n yang didop secara tidak sengaja, GaN jenis-n dan jenis-p yang didop, $Al_{0.09}Ga_{0.91}N$ jenis-n yang didop secara tidak sengaja, struktur hetero $In_{0.47}Ga_{0.53}N$/GaN jenis-n, lapisan penutup AlN/GaN). Teknik-teknik tersebut adalah pembelauan sinar-X (XRD), analisis serakan tenaga sinar-X (EDX), mikroskop imbasan elektron (SEM), mikroskopi daya atomik (AFM), pengukuran Hall, fotoluminesen (PL), dan spektroskopi Raman. Filem-filem tersebut telah dikaji dari segi ciri-ciri struktur, optik, dan elektrik.

Sejak GaN berliang adalah bahan baru, ciri-cirinya tidak kerap ditemui dalam tinjauan bacaan. Pelbagai jenis alat pencirian telah digunakan untuk mengkaji sifat-sifat morfologi, struktur dan optik bahan GaN berliang yang dijanakan melalui kaedah punaran tanpa elektrod dengan berbantukan Pt. Pelbagai sentuhan logam pada bahan GaN telah diperhati dalam projek ini untuk tujuan fabrikasi peranti. Ni didapati mempunyai ciri elektrik dan kestabilan termal yang terbaik pada suhu tinggi bagi sentuhan logam pada GaN jenis-n. Sentuhan ohmik dwi-lapisan Ni/Ag atas GaN jenis-p telah dikaji. Kerintangan sentuhan spesifik (SCRs) bagi skema dwi-lapisan ini didapati peka pada perubahan suhu dan masa penyepuhlindapan. Selain itu, kajian

sentuhan Schottky berasaskan empat jenis skema pelogaman yang berlainan, iaitu, Ti, Ag, Ti/Ag, Ag/Ti juga dilakukan pada GaN jenis-p, dan didapati rawatan haba boleh memperbaiki ciri-ciri elektrik bagi sentuhan Schottky secara amnya. Sebelum rawatan haba, ketinggian sawar (SBH) Schottky bagi Ti, Ag, Ti/Ag, dan Ag/Ti adalah 0.58, 0.71, 0.53, 0.62, masing-masing. Selepas rawatan sepuh lindap, ketinggian sawar Schottky bagi Ti, Ti/Ag, dan Ag/Ti adalah 0.67, 0.69, dan 0.66, masing-masing.

Berikutan dengan penyelidikan secara intensif kualiti bahan dan sentuhan logam, pengesan foto logam-semikonduktor-logam (MSM) berasaskan lapisan GaN berliang seterusnya difabrikasikan dan dibandingkan dengan peranti lain yang berasaskan bahan tidak berliang supaya potensi GaN berliang dapat ditinjau sepenuhnya. Kajian juga menunjukkan lapisan GaN berliang dapat meningkatkan ciri-ciri elektrik sentuhan Schottky Ni pada GaN di mana ketinggian sawar Schottky (SBH) dan kebocoran arus ini telah diperbaiki dengan berkesan. Pengesan foto berasaskan lapisan GaN berliang juga menunjukkan ciri-ciri yang memberangsangkan, di mana arus gelap yang rendah, dan nisbah arus foto kepada arus gelap yang tinggi dapat diperhatikan. Ciri-ciri fotodiod sawar Schottky ultraungu berasaskan GaN dengan lapisan penutup AlN (50nm) yang novel dibincangkan. Rawatan sepuh lindap telah menghasilkan ciri-ciri peranti yang lebih baik dengan peningkatan ketinggian sawar Schottky dan pengurangan arus gelap bagi fotodiod Schottky yang difabrikasikan. Bagi diod Schottky yang disepuh lindap pada suhu 500ºC, 600ºC, dan 700ºC, arus gelap adalah 3.25×10^{-4}, 4.97×10^{-5}, and 5.05×10^{-5} A, masing-masing, di bawah pincang 10 V. Fotodiod simpangan hetero p-GaN/n-Si telah difabrikasikan untuk pemerhatian kesan fotoelektrik.

PA-MBE GaN-BASED OPTOELECTRONICS ON SILICON SUBSTRATES

ABSTRACT

In this project, radio-frequency (RF) nitrogen plasma-assisted molecular beam epitaxy (PA-MBE) technique was used to grow GaN-based layers on Si(111) substrate using high temperature grown AlN as buffer layer. During growth, doping was done using high purity Si and Mg as n- and p-type dopants, respectively. A total of seven techniques were employed to study the properties of the GaN-based films (unintentionally doped n-type GaN, n- and p-doped GaN**,** unintentionally doped n-type $Al_{0.09}Ga_{0.91}N$, n-type $In_{0.47}Ga_{0.53}N$/GaN heterostucture, AlN cap layer/GaN). These were X-ray diffraction (XRD), energy dispersive X-ray analysis (EDX), scanning electron microscopy (SEM), atomic force microscopy (AFM), Hall measurements, photoluminescence (PL) and Raman spectroscopy. The films were evaluated in terms of structural, optical and electrical properties.

Since porous GaN-based materials on silicon substrates are a new type of material, the properties are hardly found in the literature. Several different characterization tools have been used to investigate the morphological, structural, and optical properties of porous GaN produced by Pt assisted electroless etching methods. Different features metal contacts on GaN materials have been investigated in this project for the purpose of device fabrication. Nickel was found to have excellent electrical properties and thermal stability at elevated temperatures among the metal contacts on n-type GaN. A Ni/Ag bi-layer ohmic contact on p-GaN has been explored. The specific contact resistivities (SCRs) of this bi-layer scheme were observed to be sensitive to the change of annealing temperatures and durations. Other than that, the study of Schottky contacts based on four different metallization

schemes, Ti, Ag, Ti/Ag, and Ag/Ti were performed on p-type GaN, and heat treatment was found able to improve the electrical properties of Schottky contacts generally. Before heat treatment, the Schottky barrier heights (SBHs) of Ti, Ag, Ti/Ag, and Ag/Ti were determined to be 0.58, 0.71, 0.53 and 0.62 eV, respectively. After annealing, the SBHs of Ti, Ti/Ag, and Ag/Ti were found to be 0.67, 0.69 and 0.66 eV, respectively.

Following the intensive investigations of material quality and metal contacts, metal-semiconductor-metal (MSM) photodetectors based on porous GaN-based materials were subsequently fabricated and compared to other non-porous-based devices so that the potential of porous GaN-based materials could be fully explored. The study also showed that porous GaN layer was able to enhance the electrical properties of Ni Schottky contacts on GaN in which the SBH and leakage current were improved significantly. Photodetector fabricated from porous GaN layer also showed promising properties in which low dark current and higher photocurrent to dark current ratio were observed. The characteristics of novel GaN-based ultraviolet (UV) Schottky barrier photodiodes with AlN cap layer (50 nm) were presented. Thermal annealing treatment has resulted in improved device characteristics by enhancement of Schottky barrier height, and suppression of dark current of the fabricated Schottky photodiodes. For Schottky diodes annealed at 500 ºC, 600 ºC, and 700 ºC, the dark currents were 3.25×10^{-4}, 4.97×10^{-5}, and 5.05×10^{-5} A, respectively, under 10 V applied bias. The p-GaN/n-Si heterojunction photodiode was fabricated to observe the photoelectric effects.

CHAPTER 1

INTRODUCTION

1.1 General properties of III-V nitrides

Due to their superior electrical and optical properties, the group III-nitride family, consisting of gallium nitride (GaN), aluminium nitride (AlN), indium nitride (InN), their alloys and heterostructures, primarily AlGaN/GaN and InGaN/GaN, are the subject of intense research activity worldwide as they promise to usher in a new era in optoelectronics (Sawyer et al., 2008, Razeghi et al., 1996, Strite et al., 1992).

Characteristics, such as high mobility, high breakdown voltage, high electron saturation velocity, high thermal conductivity, chemical inertness, mechanical stability, make the nitride family of semiconductors materials of choice for the fabrication of electronic devices capable of operating at high temperatures, high frequency and high power densities (DeCuir et al., 2008, Pearton et al., 1999, Sze, 1990). The nitrides can crystallize in either zinc-blend or the wurtzite form, with the wurtzite structure being the most commonly studied.

GaN is a direct and wide band gap (3.4 eV) semiconductor and when alloyed with InN (0.7 eV) (Shih et al., 2008, Jamil et al., 2008, Biju et al., 2008, Wu et al., 2002) and AlN (6.2 eV), a spectrum from infrared (IR) to ultraviolet (UV) can be covered (Strite et al., 1992). A graph illustrating the band gap and lattice constant of some of the most important compound semiconductor materials is presented in Fig. 1.1.

Unlike silicon carbide (SiC), another widely studied large band gap semiconductor with demonstrated n- and p-type doping and excellent power device performance, one advantage of GaN as well as III-V nitrides is that they form direct band gap heterostructures, have better ohmic contacts and heterostructures, which

eventually made III-V nitrides or GaN a more promising candidate than SiC in terms of application devices in optoelectronics. The transparency of high quality GaN at wavelengths longer than the band gap make it an ideal material for fabricating photodetectors capable of rejecting near infrared and visible regions of the solar spectrum while retaining near unity quantum efficiency in the UV. Besides, in optoelectronics, GaN is primarily of interest for its potential as a blue and UV light emitter (Strite et al., 1992).

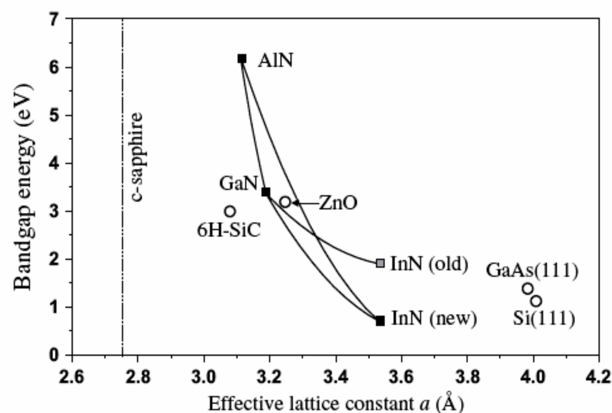

Fig. 1.1: Bandgap energy versus effective lattice constant of nitride material. (Popovici and Morkoc, 2000)

GaN-based devices are now present on the market, but much work is left in order to expand the application pool and improve the performance and reliability. Major research issues include: choice of substrate, GaN bulk and thin film crystal growth, heteroepitaxy, buffer layers, doping, contacts, etching, and integration with other semiconductors. Growth of bulk GaN crystals (ingots at least few inches in diameter) is a challenge due to their high melting temperature, very high equilibrium nitrogen vapor pressure at moderate temperatures, and low solubility in acids, bases and most other inorganic elements and compounds. Since no large bulk GaN is available at this time, the future industrialization of these wide bandgap compound

materials depends on the development of high-quality heteroepitaxial growth techniques on various substrates. Due to the need to understand, predict and optimize the growth process of the GaN films, work is needed to understand the heteroepitaxy growth of GaN.

1.1.1 Crystal structure of group III-nitrides

The table in Appendix A summarizes the fundamental properties of wurtzite III-nitride semiconductors at room temperature. The group III atoms form compounds with N that have a composition of III-N. These compounds have four covalent bonds with four tetrahedral bonds for each atom. This is depicted schematically in Fig. 1.2. Such bonds make a significant ionic contribution because of the large differences in electronegativity of the two constituents. The GaN can crystallize in two crystalline phases: wurtzite which has hexagonal symmetry and is the thermodynamically equilibrium phase, and zinc-blende which is cubic. The hexagonal wurtzite GaN with a direct band gap of 3.4 eV is the most-studied material among all group III nitrides. The lattice parameters of the wurtzite hexagonal GaN are: a = 3.1892 ± 0.0009 Å, and c = 5.1850 ± 0.0005 Å (Maruska et al., 1969, Detchprohm et al., 1992).

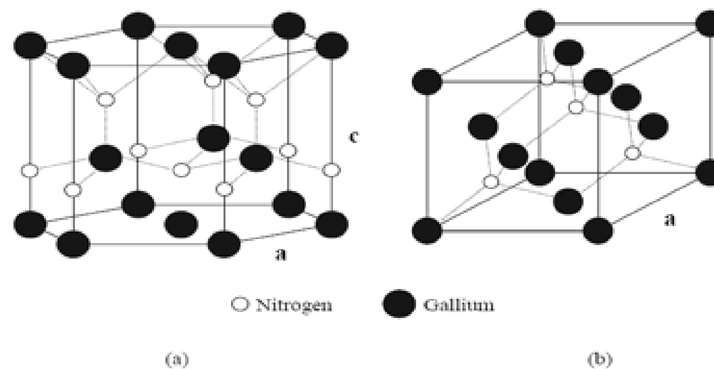

Fig. 1.2: The (a) wurtzite structure, and (b) zinc blende structure of III-V nitrides. (Detchprohm et al., 1992)

1.1.2 Brief history of the group III-nitrides

III-nitride semiconductors have been studied for more than a half century. In 1928, Tiede et al. first reported AlN growth (Tiede et al., 1928). Following that, Johnson et al. in 1932 reported the synthesis of GaN by passing ammonia over hot gallium (Johnson et al., 1932). This method produced small needles and platelets. Their purpose was to study the crystal structure and lattice constant of GaN as part of a systematic study of many compounds.

Two decades later, Grimmeiss et al. (Grimmeiss, et al. 1959) used same technique to produce small GaN crystals for the purpose of measuring photoluminescence spectra. The synthesis of InN was reported by Juza in 1938 (Juza et al., 1938). A breakthrough occurred in 1969, when Maruska (Maruska et al., 1969) succeeded in growing the first single-crystal GaN on sapphire substrate by hydride vapor phase epitaxy (HVPE). All the GaN made at that time was very conducting n-type even when not deliberately doped. They found that GaN possesses a direct transition band structure with bandgap energy of about 3.39 eV.

In 1971, the first metal-insulator-semiconductor (MIS) light emitting diode (LED) was demonstrated but until 1989, only few publications and improvements of GaN have been published. Since 1992 up to now, the research and development activities in the field of the group III nitrides rapidly increased. From the double heterostructure (DH) LED and laser diode (LD) up to the high electron mobility transistor (HEMT), all devices could be realized with the nitrides. Metal-organic chemical vapor deposition (MOCVD), also called metal-organic vapor phase epitaxy (MOVPE), is the favorite growth method for the epitaxial layers. Besides this, molecular beam epitaxy (MBE) is also used.

1.1.3 Doping of GaN

Doping with atoms that have more or less valence electrons than gallium is employed to control the electrical properties of GaN films. Nominally as grown GaN thin film has intrinsic n-type carriers and the doping level is normally higher than 10^{16} cm^{-3}. This n-type doping is generally caused by nitrogen vacancies (V_N) in the crystalline structure, which are expected to be shallow donors in GaN films. Oxygen is commonly found as an impurity in GaN layers, and contributes to the n-type carrier concentration (Seifert et al., 1983, Chung et al., 1992).

The most common n-type dopant in GaN is silicon (Si). Controllable silicon doping of GaN has been demonstrated over a wide range of concentrations (low 10^{17} cm^{-3} to mid 10^{19} cm^{-3}). Several groups have shown linear increase of the electron concentration with the silicon/gallium ratio using Van der Pauw Hall measurement at 300 K (Nakamura et al., 1992a, Rowland et al., 1995, Kadena et al., 1996). As the electron concentration is increased, there is also the decrease in the electron mobility due to impurity scattering. Although high electron concentrations can be achieved with silicon doping, cracking of GaN films grown on sapphire has been observed (Murakami et al., 1991). High Si doping levels provide for a low resistance ohmic contact to the n-type GaN for LEDs. Recently Burm et al. have shown that a shallow Si implant at a dose of 1×10^{18} cm^{-2} to produce a doping density of 4×10^{18} cm^{-2} followed by an 1150 °C anneal for 30 sec results in very low contact resistance of 0.097 Ωmm and a specific contact resistance of 3.6×10^{-8} Ωcm^2 (Burm et al., 1997).

p-type doping of GaN has proven to be significantly more challenging because the fact that the as grown GaN film is as intrinsically n-type semiconductor. For highly efficient optoelectronic devices such as p-n junction based LEDs and laser diodes, p-type doping level is a critical parameter. For p-type doping, magnesium

(Mg) has proven to be the most successful dopant thus far. Highly doped p-type GaN films with a doping level of 10^{18} - 10^{19} cm^{-3} have been recently achieved using elemental Mg (Moustakas et al., 1993a, Akasaki et al., 1994, Molnar et al, 1993, Nakamura et al., 1991). Magnesium occupies cation sites and is a shallow acceptor in GaN.

Other impurities have also been investigated for the purpose of finding an acceptor of GaN with smaller ionization energy, which could contribute to enhancing the p-type conductivity. Another possibility is the group II element beryllium (Be). Be is a common p-type dopant in the more conventional III-V compound semiconductors, such as GaN. The Be acceptor level was theoretically predicted to be as low as 60 meV above the valence band (Bernardini et al., 1997). Up to now, Zn, C, Ca and Be have been tested, but Mg is still recognized as the best p-type dopant of GaN crystals.

When metal organic chemical vapour deposition (MOCVD) is used as the growth method, a postgrowth annealing is necessary because it was found that hydrogen neutralizes the Mg acceptor. The postgrowth annealing is carried out at temperatures of 700 °C and 900 °C (Akasaki et al., 1994) or by using a low energy electron beam (LEEBI) process (Amano et al., 1989). During postgrowth treatment, the Mg-H bond is broken, thus forming an electrically active Mg center. However, if there is any atomic hydrogen present, the Mg-H complexes will reform and the sample will remain highly resistive. The as grown GaN film by molecular beam epitaxy (MBE) does not have the neutralization effect by hydrogen because the MBE does not use the hydrogen source. The highest hole concentration achieved by MOCVD and MBE are 3.0×10^{19} cm^{-3} (Svensk et al., 2007) and 4.7×10^{18} cm^{-3} (Burnham et al., 2008), respectively.

1.2 GaN-based optoelectronics on silicon substrates

For the last 15 years silicon as a substrate has attracted much attention for the epitaxial growth of III-V compounds like GaAs and InP because of its low price and its availability in large diameters up to 12 inches now. However, in spite of huge efforts, no real breakthrough has been obtained because of the high density of dislocations in these materials leading to a rapid degradation of all devices fabricated so far. In contrast, GaN-based devices are known to operate very well without aging effects with dislocation densities as high as 10^{10} cm^{-2}. Thus, the integration of Si- and GaN-based devices on the same chip becomes feasible as well as a silicon based optoelectronics technology, with the potential for small, high resolution, full color displays.

From the point of view of economics, Si offers a low price as compared to sapphire and SiC, high crystalline perfection, availability of large size substrates, all types of conductivity, and high thermal conductivity (1.5 W cm^{-1}). In most cases the Si(111) plane is chosen because of its trigonal symmetry favoring epitaxial growth of the GaN(0001) plane. The large difference in the lattice parameters of GaN (a_{GaN} = 0.31892 nm) and Si ($a_{Si(111)}$ = 0.38403 nm) yields a lattice parameter mismatch of 16.9 % resulting in a high dislocation density of ~ 10^{10} cm^{-2} which is comparable to GaN on sapphire.

The most severe problem is the large thermal mismatch between GaN and Si. The in-plane thermal expansion coefficient of GaN is 5.59 x 10^{-6} K^{-1} (Maruska et al., 1969) as compared to 3.77 x 10^{-6} K^{-1} of Si (Okada et al., 1984), which leads to a large tensile stress during cooling from the growth temperature to room temperature often resulting in cracked layers preventing device applications. The tensile stress causes a concave bending of the film/substrate system.

1.2.1 LEDs on silicon substrates

The first GaN-based light emitting diode on Si substrate was reported by Guha et al. (Guha et al., 1998). The double heterostructure was grown by MBE on n-type Si(111) with an intermediate 8 nm AlN buffer. The structure consisted of n-$Al_xGa_{1-x}N$/6 nm GaN (Si-doped or undoped) as an active layer/p-$Al_xGa_{1-x}N$/15 nm p-GaN layers with $0.05 < x < 0.09$. Ni/Au thin (14 nm) transparent metals served as p-type contacts and electron injection was carried out from the backside through the Si substrate.

The diodes start light emitting at 4.5 - 6.5 V with reverse leakage currents from 10 to 130 μA at -10 V. At 12 V, the forward currents varied from 14 to 65 mA. These rather high values as compared to MOVPE grown devices on sapphire or SiC were attributed to a low p-type doping and non-optimal p contacts. A device with a Si-doped thin GaN layer showed a near band edge electroluminescence at 360 nm with a full width at half maximum of 17 nm, and a broad long wavelength tail that extended out into the visible spectral range, while a heterostructure with an undoped GaN layer showed a broad emission band centered at 420 nm most probably due to deep radiative levels in the gap.

The same authors reported on multicolored light emitters on silicon substrates using similar violet MBE grown GaN LEDs as described above with somewhat higher Al-content ($x = 0.15$). In conjunction with organic dye based color converters orange at ~ 600 nm and green-yellow at ~ 530 nm, electroluminescence on the same Si wafer is obtained. The output power was not given but the 'visible part of the electroluminescence was bright enough to be clearly observed by the eye under normal room illumination'. It should be noted that the layers showed cracks.

Tran et al. reported the growth of InGaN/GaN multiple quantum well (MQW) blue LEDs on Si(111) grown by MOVPE (Tran et. al., 1999). The structure consisted of a 20 nm AlN buffer deposited at 750 ºC, 4 μm n-doped GaN, an undoped ten period MQW (2 nm $In_{0.22}Ga_{0.78}N$/9 nm GaN), a 40 nm p-doped $Al_{0.1}Ga_{0.9}N$ layer and 0.3 mm p-GaN cap layer. The structure showed blue electroluminescence at 465 nm. Light emission started at 4 V, the reverse leakage current was 60 mA at -10 V. An optical power output was not given. This structure showed also cracks.

Yang et al. fabricated an InGaN/GaN MQW LED by a combined MBE/MOVPE growth procedure in selective areas defined by openings in a SiO_2 mask (Yang, et. al., 2000). The density of cracks was comparable to similar structures on flat SiC substrates. For the LED, a forward turn-on voltage of 3.2 V was measured. The forward differential resistance was a factor of four higher than in comparable LEDs on sapphire substrate. At room temperature the device emitted at 465 nm.

An MBE-grown ultraviolet electro-luminescence GaN/AlGaN single hetero-junction LED on Si(111) was also reported by Sánchez-Garcia et al., (Sánchez-Garcia et al., 2000). Room temperature electroluminescence centered at 365 nm with a Full width at half maximum (FWHM) of 8 nm was obtained. The turn-on voltage was 5 V, the structure suffered from a reverse leakage current of 200 μA at -5 V. The optical ultraviolet output power was estimated to be 1.5 mW at 35 mA.

1.2.2 Lasers on silicon substrates

The recent surge of interest and research activity in Si-based lasers highlights the potential benefits that full capability in photonics could bring to the Si world. Some of the recent advances in lasing are based on emission from rare earth (RE)

elements contained in GaN heteroepitaxially grown on Si. This approach has led to the first demonstration of visible lasing on Si. The eventual success of this approach will result in the availability of laser light sources built directly on Si substrates and operating at wavelengths throughout the visible and near-infrared (IR) range.

The use of light for improving the performance and flexibility of Si microelectronics has been an elusive goal for many years. Long-haul telecommunications has clearly made the transition to optical technology, driven primarily by the wider bandwidth available in silica glass fibers. The next optical revolution is in computation capability. As computer processor speeds continue to increase, computing performance is increasingly limited by data rates between the main processor and its environment. These include connections between processors, and peripheral devices, etc.

Optical domain communication offers many important attributes, such as increased bandwidth, increased transmission path, reduced signal cross-talk, reduced sensitivity to electromagnetic interference, and reduced weight. If achieved, the integration of electronics and photonics on a single Si substrate will result in the development of on-chip optoelectronics incorporated with electronic circuits and optical devices. This, in turn, would provide much greater functionality and performance compared with existing purely microelectronic circuits. The building blocks required for integrated Si-based optoelectronics include an appropriate light source, on-chip optical modulator, and photodetector. Of these, clearly the most challenging element is the need for a Si-based laser.

The first successful demonstration of visible (at ~ 620 nm) lasing on Si was achieved by optical pumping of Eu-doped GaN epilayers, with unique AlGaN transition layers, grown on Si substrates by solid-source molecular beam epitaxy

(MBE). The initial results are very encouraging with a measured stimulated emission threshold of only ~ 110 $kWcm^{-2}$, optical gain of ~ 100 cm^{-1}, and loss of ~ 45 cm^{-1}. These results provide strong evidence that injection lasers based on AlGaN-GaN:RE-AlGaN double heterojunction structures grown on Si substrates are feasible.

Fig. 1.3 displays the materials used in the demonstrations to date of lasers on Si and the corresponding wavelength and emission color. The wavelength scale also indicates emission obtained from various REs in GaN. The insert to Fig. 1.3 is a photograph of stimulated emission from a GaN:Eu thin film on Si that is optically pumped. The approach to achieving a versatile Si-based laser system using RE-doped GaN films grown on Si substrates is founded upon the combination of few key factors: (i) robust, optically efficient, wide bandgap semiconductors: LEDs and laser diodes (LDs) based on GaN, along with alloys of AlN and InN, have been developed to a very high degree of efficiency despite the absence of a native III-N substrate. Typically, sapphire, which has a significant lattice mismatch to GaN, is used as a substrate leading to a large defect dislocation density in the epilayers. However, light emission in the III-N epilayers is very strong and intrinsic lasing (i.e. near-bandgap) from GaN-on-Si structures has been reported (Bidnyk et al., 1998). In addition, Yablonskii et al. have reported stimulated emission from GaN at near UV wavelengths (~ 368 nm) using optical pumping at 337 nm (Yablonskii et al., 2002). (ii) efficient RE-doped GaN devices: the use of GaN (and AlGaN) as host materials for different RE ions has been developed and efficient electroluminescent devices (ELDs) with emission at many wavelengths from the visible to the IR have been demonstrated. ELDs have been grown on both sapphire and Si substrates. More recently, stimulated emission has been obtained from Eu-doped GaN structures fabricated on Si substrates.

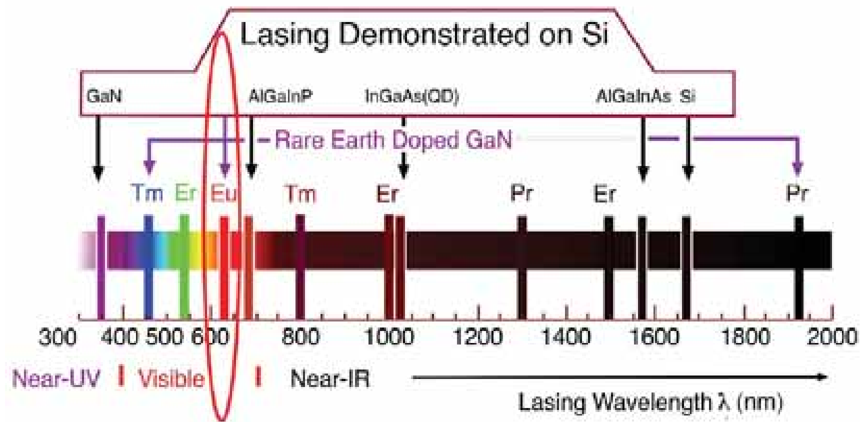

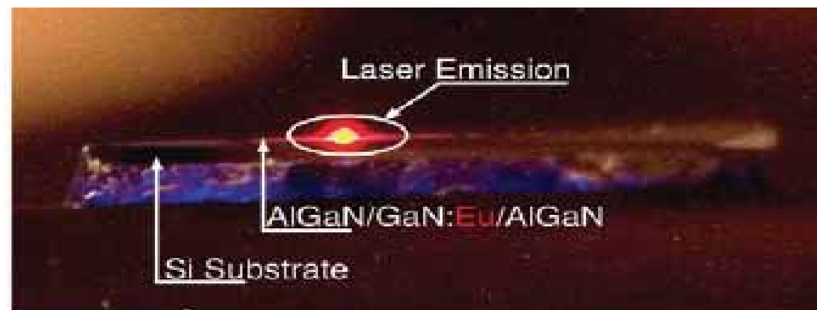

Fig. 1.3: Materials used in the demonstrations to date of lasers on Si and associated wavelength and emission color. Wavelength scale also indicates emission obtained from various REs in GaN. (Steckl et al., 2007)

1.2.3 Photodetectors on silicon substrates

High conductivity of a silicon substrate draws attention of researches to construct ultraviolet (UV) photodetectors based on surface barrier GaN/Si structures. The $Al_xGa_{1-x}N$ material system has been demonstrated to be well suited as a photodetector material for the 200 – 365 nm wavelength range. This success has led to the commercialisation of nitride-based UV photodetectors. Some of the potential uses of these UV photodetectors are endoatmospheric sensing of jet or rocket plumes, of solar UV rays, and for flame detection. Requirements for these photodetectors include high visible rejection, high responsivity, and linearity and low time response.

Silicon substrate presents the obvious advantages of a well known technology, low cost and potential hybrid integration. However, Si(111) has been less

investigated than sapphire as a substrate to grow nitrides, due to the higher lattice and thermal expansion coefficient mismatches which produce a higher dislocation density and the potential generation of cracks. In addition, the problem of the interdiffusion at the Si/epilayer interface makes the interpretation of electrical measurements more difficult. There are only a few reports on GaN photodetectors on Si(111), including photoconductors and Schottky photodiodes (Chiou et al., 2008, Wang et a., 2006). The performance of these devices was poor in comparison with photodetectors on sapphire.

1.3 Research objectives

GaN-based or the III-V nitrides materials are wide band gap semiconductor materials with potential applications in optoelectronic as well as in electronic devices operating at high power and high temperature conditions. Although the research on GaN is actively being investigated around the world for its significance, but the research on these materials is new in Malaysia.

In metalorganic chemical vapor deposition (MOCVD), chemical reaction takes place by intercepting different gases flow on a heated surface with high growth rate; this method has been widely applied in commercialization. However, for research purposes, most III-nitrides are grown by molecular beam epitaxy (MBE) to control growth rate and thickness to a great accuracy. MBE is a low temperature alternative to growth processes such as MOCVD. MOCVD growth temperatures for GaN are typically in excess of 1000 ºC, while MBE temperatures are usually in the range of 700 - 800 ºC. This allows for more flexibility in the choice of substrate materials and minimizes thermal effects such as diffusion. Growth rates are typically about 0.3 to 1 μm/hr. This allows thickness control on the atomic level. All of these

factors combine to help MBE exhibit extremely fine control over semiconductor growth. With this control, MBE has made a tremendous impact on the world of device fabrication. Both optical and electronics devices have been aided greatly by use of the MBE technique. MBE continues to be uniquely suited to the growth of many device structures.

The main objective of this project is to use radio-frequency (RF) nitrogen plasma-assisted molecular beam epitaxy (PAMBE) technique to grow high quality GaN-based materials on Si(111) substrate for exploration of the potential of these materials for optoelectronics applications. The studies of metal contacts on GaN-based materials are also important research areas which will give an insight in the GaN-based device technology. In this work, a variety of metal contacts on n- and p-type GaN-based materials have also been investigated to study the change of electrical, morphological properties and thermal stability of the contacts under different environments.

Besides that, tremendous effort is channeled into the exploration of the fundamental properties of the porous GaN-based materials on silicon substrates; a new form of material which is not much reported in the literature, therefore, in this project, works have been devoted to the study of the structural, morphological, optical and electrical properties of this material. Following the intensive investigations of material quality and metal contacts, metal-semiconductor-metal (MSM) photodetector based on porous GaN-based material are also fabricated and compared to other non-porous-based devices so that the potential of porous GaN-based material could be fully explored.

1.3.1 Originality of the research works

High quality GaN-based layers were grown on Si(111) substrates by radio frequency (RF) nitrogen plasma-assisted molecular beam epitaxy (PAMBE). The growth of III-nitrides on Si(111) was initiated with a previous coverage of Al to avoid the formation of amorphous Si_xN_y. The two-step growth of AlN films as buffer layer has been carried out. The first step is a short high temperature deposition. Typically, this AlN buffer layer deposition was started by Al cell temperature at 1161 °C (Al high flux of 3.50 x 10^{-7} Torr BEP). Then Al cell temperature was then decreased to a lower temperature, typically 1120 °C (Al low flux of 1.20 x 10^{-7} Torr BEP). In addition to AlN high crystal quality as buffer layers, a very flat surface was required in order to achieve a two-dimensional (2D) GaN-based growth.

During growth, doping was done using high purity Si and Mg as n- and p-type dopants, respectively. From the literature, the highest p-type doping concentration was measured to be (3-7)x10^{19} cm^{-3} by MOCVD (Svensk et. al., 2007). In this work, a p-type carrier concentration of GaN as high as (4-5)x10^{20} cm^{-3} was obtained by PAMBE without post growth annealing treatment. The investigation of light emitting Schottky diodes based on p-GaN/Si(111) has also been carried out.

For the porous GaN-based material on silicon, the use of porous GaN-based layer for improving the electrical characteristics of nickel (Ni) Schottky contacts; and the fabrication and investigation of various devices based on porous GaN-based layer in this project, which were MSM photodetector on silicon substrates, have not much been reported in the literature. The characteristics of novel GaN-based ultraviolet (UV) Schottky barrier photodiodes (PDs) with AlN cap layer (50 nm) was presented. Although AlN is a wide band gap semiconductor, its properties are like

those of an insulator with a high dielectric constant, good conductivity, and large breakdown electric field. Therefore, AlN may be a good insulator for blocking the leakage current.

1.4 Outline of the thesis

The next chapter, Chapter 2, will cover an overview of the GaN technology, such as the III-V nitrides growth techniques, factors influencing the GaN crystalline quality, III-V nitrides based photodetectors, metal-GaN contact technology, and the development of porous GaN-based material. Chapter 3 is devoted to the salient features of a typical MBE system, which includes an introduction to the MBE radio frequency (RF) plasma nitrogen source, vacuum chamber, effusion cells, and the sample manipulation, followed by a discussion of the growth rate and the GaN surface morphology phase diagram under different growth condition. In Chapter 3, the basic principles of characterization tools, process equipment, and porous GaN formation mechanisms are presented. Methods in studying material properties, metal contacts, porous GaN-based as well as the fabrication and characterization of various types of devices are also covered in Chapter 4.

The results obtained from the research works are analyzed, discussed in Chapters 5, 6, 7, and 8. Chapters 5 and 6 are devoted to the study of GaN material quality and the properties of the porous GaN. Chapter 7 is devoted to the study of metal contacts on GaN, and Chapter 8 reports the performance of the devices fabricated based on porous and as-grown GaN-based material. The final Chapter 9 concludes the thesis with a summary of the research work. Conclusion of the results obtained and a few suggestions for future research are included.

CHAPTER 2

LITERATURE REVIEW

2.1 III-V nitrides growth techniques

Since no traditional method of bulk crystal growth is capable of making large size GaN single crystals, researchers have concentrated their efforts on obtaining good quality GaN thin films on various substrates. A number of growth methods have been investigated for the crystal growth of III-V nitride thin films. Nevertheless, recent improvements have made molecular beam epitaxy and metalorganic chemical vapour deposition the key methods for the growth of GaN.

2.1.1 Molecular beam epitaxy (MBE)

Epitaxy has its word origin from Greek and means "ordered on top". Molecular beam epitaxy can be dated back to the year 1958 when Gunther (Gunther et al., 1958) described a technique of growing compounds on heated substrate by evaporation from two sources. The major developments towards modern MBE equipment were made by Cho and Arthur in 1975 (Cho et al., 1975). The growth chamber is the heart of an MBE system (Fig. 2.1). It consists of Knudsen effusion cells, shutters, a continuous azimuthally rotation substrate holder, beam flux ionization gauges, liquid nitrogen shrouds and one in-situ characterization method, which is reflection high energy electron diffraction (RHEED).

During the growth process, elemental sources are heated in Knudsen cells and evaporated at controlled rate onto a heated substrate under ultra-high vacuum (UHV) conditions ~ 10^{-10} – 10^{-11} Torr. The UHV growth environment is crucial to the MBE process. It provides an ultra clean growth ambient leading to epitaxial layers with

the highest purity. This is extremely important for growing high quality semiconductor materials which are used for high performance devices. Under UHV condition, the long mean-free path of particles minimizes collisions or reactions between molecules in the beam, which results in a line-sight growth reaction at the surface.

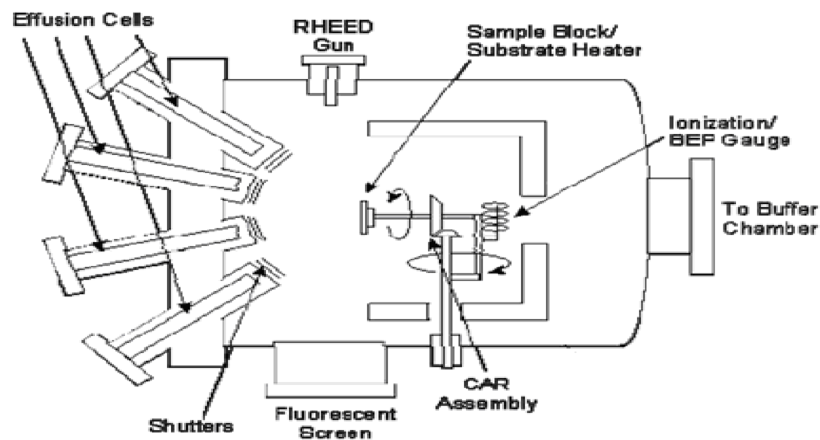

Fig. 2.1: Schematic diagram of growth chamber in a typical MBE system. (Sghaier et al., 2004)

GaN films growth by MBE are usually carried out at relatively low temperatures of 650 – 800 °C with typical growth rate of one to three monolayers per second, approximately 0.3 to 1 μm/h. On the other hand, molecular nitrogen is stable which has a strong N-N bond and does not chemisorb on a GaN surface below 950°C, due to the strong N-N bond of the nitrogen molecule. Atomic nitrogen or nitrogen containing molecule with weaker bonds should, therefore, be provided. Several modifications to conventional MBE methods have been implemented for III-N growth. Since nitrogen incorporation is difficult at low temperature when ammonia is used, plasma cells are widely used to provide the nitrogen species, which are often called plasma-assisted MBE. The generated nitrogen species is chemically

so active that the growth temperature of nitrides is low. Among them, radio-frequency (RF) or electron cyclotron resonance (ECR) plasma sources are commonly employed to activate the nitrogen species.

Nitrogen gas (N_2) is a simple, safe and clean N source, but its strong triple bond (225.1 kcal/mol) needs external activation for dissociation. The ECR source uses a microwave power (2.45 GHz) which is efficiently coupled to a nitrogen gas flow using coaxial cylindrical cavity geometry and generate a microwave discharge. The plasma stream is diffuse and neutral, providing atomic, molecular ionic and N radicals to the growth surface. The plasma source can cause degradation of the optical and electrical properties of GaN films due to the etching process that occurs at high energies. Compact RF sources (13.56 MHz) for nitrogen stream specifically designed for MBE reactors have become commercially available, and RF plasma assisted MBE is widely used for the III-nitride material growth. Employment of MBE allows reducing intrinsic thermal stress of GaN, because the film growth is carried out at relatively lower substrate temperatures (~800°C) than during MOCVD (~1200°C).

2.1.2 Metal-organic chemical vapour deposition (MOCVD)

MOCVD is a thin film growth technique which involves the flow of gaseous precursors into a reaction chamber, which will contain a heated substrate. MOCVD has appeared as the paramount nominee for commercial applications because of the accomplishment of bright blue LEDs and large scale-manufacturing potential of the MOCVD technique. Generally, CVD is a process in which high-quality thin layers of intrinsic or doped layers of semiconductors can be grown. The substrate is heated

to high temperatures where chemical decomposition, called pyrolysis of a gas, generally takes place directly on the surface of the heated substrate.

For III-V nitrides growth, MOCVD reactors combine laminar flow at high operating pressures and feature separate inlets for the nitride precursors and the ammonia to reduce predeposition reactions. Proper precursors should be used such as those possessing good reactivity, thorough pyrolisis, and transportability. Preferably, the precursors should be nonpyrophoric, water and oxygen insensitive, noncorrosive, and nontoxic. Trimethylgallium (TMG) and triethylgallium (TEG) are very popular for Ga, though GaCl has been tried. Trimethylindium (TMI) and trimethylaluminium (TMA) are the commonly employed sources of In and Al, respectively. Ammonia (NH_3) is considered the best source of nitrogen, as it is reasonably pure and stable. Precursors are transported to the growth chamber using hydrogen carrier gas and are injected into the reaction chamber. The gas manifold typically features fast switching of the group III elements and dopants, and permits the separate injection of ammonia. Fig. 2.2 is a schematic representation of an atmospheric-pressure reactor, with the optional low-pressure capability.

Normally c-plane (0001) oriented sapphire substrates are used, although other orientations of sapphire and alternative substrates are sometimes employed too. In the MOCVD reactor, TMG, TMA, or TMI reacts with ammonia at the substrate which is heated to about 1000 °C where the common feature here is that the reactants must be allowed to interact with one another only on the surface of the substrate. To obtain high quality single crystalline GaN films, temperatures in excess of 800 °C are required. However, the best GaN films are grown at 1050 °C. The dissociation of GaN results in voids in the grown layer which can happen at substrate temperatures exceeding 1100°C where a similar situation has also been observed for AlN film

growth. N_2H_4 has been employed instead of NH_3 as a way to overcome this problem because a significantly smaller amount of N_2H_4 was required to maintain the same growth rate. On the other hand, a lower deposition temperature of III-V nitrides can be achieved by utilizing an activated form of nitrogen. This new CVD technology is interesting as the deposition of amorphous and polycrystalline GaN films at deposition temperatures lower than 300 °C can be accomplished by plasma-enhanced CVD. Other methods that use the same principle of nitrogen activation to grow III-V nitrides are like laser-assisted CVD, remote plasma-enhanced CVD, photo-assisted CVD, and electron cyclotron resonance (ECR) plasma-assisted CVD.

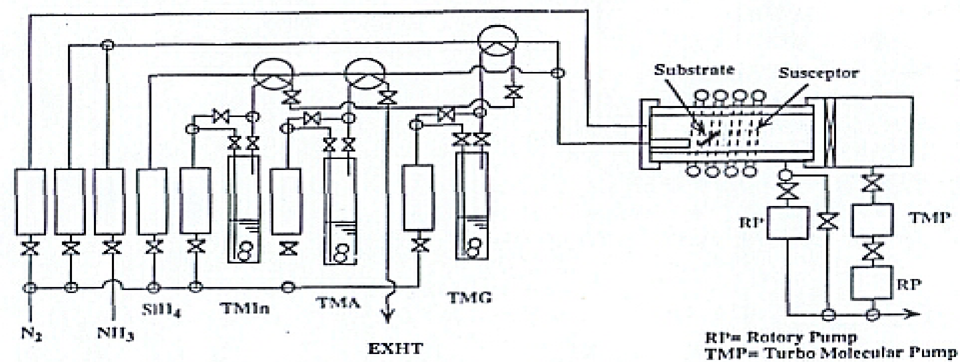

Fig. 2.2: Diagram of a horizontal MOCVD reactor. (Morkoc, 1999)

2.2 Factors influencing GaN crystalline quality

Bulk GaN crystals are not commercially available for industrial use. The only substrates which are close to bulk GaN substrates are thick epitaxial GaN layers e.g. on sapphire. The US-based company "Technologies and Devices International, Inc (TDI)" offers up to 25 μm thick GaN layers on sapphire grown by MOVPE and HVPE. The France-based company "LUMILOG" offers among others 400 μm thick free-standing 2" GaN substrates which were grown on sapphire.

Nevertheless, the development of thick GaN layers as substrate material is still at the beginning and therefore most of the researchers are limited to heteroepitaxy. One of the superior problems rests with the lack of well-suited substrates, since GaN single crystals of sufficiently large dimensions are not yet available, hence GaN film has to be grown heteroepitaxially on foreign substrates, this leads to the generation of high density of structural defects. Nevertheless, the utilization of low temperature buffer layer joined with the advancement of epitaxial growth techniques consent great enhancement in the crystalline quality and subsequently the reduction of the high background electron density in GaN, these lead to an enormous improvement of carrier mobility and finally the performance of GaN-based devices.

2.2.1 Substrates

III-V films have been grown heteroepitaxially on a number of substrates that share more or less similar lattice constants and thermal expansion coefficient of III-nitrides. There are no ideal substrates for heteroepitaxy of GaN. It is for that reason; the nitride growth on different substrates will be discussed in this section.

Table 2.1 shows the lattice constant and thermal expansion coefficient for some prospective substrates as compared to nitrides. The density of threading dislocation defects in GaN films as high as 10^{10} cm^{-2} have been reported and they are undesirable for many applications especially laser diodes where the emission is due to a bound exciton. These defects originate from the substrate/GaN interface and propagate into the epilayer. The large difference of lattice constant and thermal expansion coefficient between the substrate and GaN is considered to be the major factor attributing to the high density of this defect. Sapphire exhibits a higher thermal

expansion coefficient relative to GaN, and for 6H-SiC, the thermal expansion coefficient is smaller than GaN. GaN films grown on sapphire and 6H-SiC will experience compressive and tensional biaxial strain respectively (Monemar et al., 1997). However, with the formation of threading dislocations, the strain in the GaN epilayer will be released.

Table 2.1: Lattice parameters and thermal expansion coefficient of substrates (Popovici and Morkoc, 2000)

Crystal	Symmetry	Lattice constant (nm) (a; c)	Thermal expansion coef. (a; c) ($\times 10^{-6}K^{-1}$)
Al_2O_3	Hexagonal	(0.4758; 1.299)	(7.5; 8.5)
ZnO	Wurtzite	(0.3250; 0.5213)	(8.25; 4.75)
6H-SiC	Wurtzite	(0.308; 1.512)	(4.2; 4.68)
InP	Cubic	0.5869	4.5
MgO	Cubic	0.4216	10.5
3C-SiC	Cubic	0.436	-
Si	Cubic	0.54301	(3.59)
GaAs	Cubic	0.56533	6
GaN	Wurtzite	(0.3189; 0.5185)	(5.59; 3.17)
GaN	Cubic	0.452	-
AlN	Wurtzite	(0.3112; 0.4982)	(4.2; 5.3)
InN	Wurtzite	(0.353; 0.569)	-

The linear expansion coefficient for cubic is not available. However, since only the second nearest neighbor distance and only in the *c* direction, differs between the wurtzitic and cubic phases, we can assume that the linear expansion coefficient for the cubic phase will be in the same bulk part as in the wurtzitic phase.

Sapphire (Al_2O_3) having a different lattice constant and thermal expansion coefficient from GaN, it is still the most commonly used substrate for GaN growth because of its hexagonal symmetry, wide availability, and ease of handling and pre-growth cleaning. Sapphire is stable at high temperature, which is typically required

for GaN film grown by MOCVD method. Besides that, sapphire is also electrically insulating, therefore, all electrical contacts have formed on the front side of the device, reducing the area available for devices and complicating the device fabrication (Liu and Edgar, 2002).

6H-SiC shows a closer lattice constant and thermal expansion coefficient to GaN, but, this substrate is high-priced. GaAs has been used as substrate regardless of its poor compatibility. This is mostly due to its widely availability and familiarity of the researchers. Other uncommon substrates such as ZnO, and MgO (Popovici and Morkoc 2000), also have been used as substrate, however, there are not much technical information available in the literature, therefore, the use of these substrates need to be further explored. Lattice mismatch between GaN and the most commonly used substrates is summarized in Table 2.2. The type of strain caused by the mismatch is denoted by the positive and negative signs (negative sign: compressive strain; positive sign: tensile strain).

Table 2.2: Lattice mismatch between GaN and the substrates.

Substrate	Lattice mismatch (%)	Reference
Si(111)	+17	(Tansley et al., 1997)
Si(001)	+17	(Tansley et al., 1997)
3C-SiC	-4	(Tansley et al., 1997)
GaAs(100)	+20	(Tansley et al., 1997)
GaAs(111)	+20	(Tansley et al., 1997)
Al_2O_3(0001)	+16	(Kung et al., 1994)
6H-SiC(0001)	-4	(Tansley et al., 1997)